RSC Advances

PAPER

View Article Online
View Journal | View Issue

Cite this: *RSC Adv.*, 2020, **10**, 14877

Nitric oxide sensors using nanospiral ZnO thin film deposited by GLAD for application to exhaled human breath

Pingxiang Luo,†[a] Min Xie,†[a] Jingting Luo,*[b] Hao Kan[b] and Qiuping Wei[c]

ZnO is a promising gas sensing material for its excellent gas sensing response characteristics and long-term stability. Moreover, the improvement in the sensitivity and response speed of ZnO gas sensors can be achieved by the nanostructure fabrication. This paper proposes a facile method to deposit ZnO nanospirals using glancing angle deposition (GLAD) for application in nitric oxide (NO) sensors. ZnO nanospirals with porous characteristics have larger relative surface area and more active surfaces, compared with dense ZnO thin film. A sensor using nanospiral ZnO film shows a response factor of 16.9 to 100 ppb NO at 150 °C in 40% RH, which is 3 times larger than that of the sensor using dense ZnO film. Such a ZnO nanospiral sensor system can detect NO as low as 10 ppb which is below the NO concentration (>30 ppb) in exhaled breath of patients with asthma. The effects of working temperature and humidity on the sensor performance were investigated systematically in this work. Moreover, the sensor response showed a good selectivity to NO and high stability as the time increased up to 24 days. NO gas sensing mechanism was discussed in detail and nanospiral ZnO film sensors are promisingly applicable for exhaled human breath application compared with some other NO sensors.

Received 16th January 2020
Accepted 23rd March 2020

DOI: 10.1039/d0ra00488j

rsc.li/rsc-advances

Introduction

There is extensive research on developing sensitive and selective nitric oxide (NO_x) gas sensors for applications in the fields of high temperature combustion, environmental protection and clinical analysis.[1–4] In the clinical analysis application, nitrogen monoxide (NO) concentration in exhaled human breath is a biomarker for pulmonary inflammation processes of the lower respiratory tract, *e.g.* asthma.[5–7] Normally, the amount of NO in exhaled breath of a healthy human being is below 10 ppb.[8,9] However, in the case of an asthma patient due to inflammatory response in the airways, which is especially serious for young children, the NO concentration in the exhaled breath can increase up to 100 ppb.[10,11] In general, human exhaled breath is a mixture of N_2, CO_2, NO_x, NH_3, CO, and hundreds of volatile organic compounds with concentrations ranging from several ppt to ppm.[12–14] Regarding the complexity, breath analysis needs a NO sensing material with high sensitivity which is able to detect NO concentrations in the range of 1 to 100 ppb, and is selective against the above exhaled breath mixture in a highly humid environment (relative humidity (RH) > 80%).

Due to the stability, good sensing response characteristics and possibility for low-cost and mass fabrication, metal-oxides, such as SnO_2,[15] In_2O_3,[16] WO_3 and Cr_2O_3 (ref. 17–19) *etc.* are widely used as sensing materials for NO gas sensing in recent years. However, the limit of detection (LOD) of NO gas in human breath using these metal oxide-based sensors still needs improvement.[20–22] Assembling sensing materials into porous and nano-sized structures to form active surfaces is an effective method to enhance the sensitivity, selectivity, as well as the response and recovery speed of NO gas sensors.[23–25] However, to explore large-scale synthesis technology of nanostructures with a specific morphology by a controllable and reproducible chemical route, and to establish the relationship between a specific nanostructure and its physicochemical properties, are always challenging.

ZnO is an ideal NO gas sensing material with a wide energy band gap (3.3 eV), and the advantage that the selectivity, the sensitivity and the response time can be improved by fabricating porous nanostructures thin films using glancing angle deposition (GLAD).[26,27] GLAD technology can grow nearly arbitrary shaped nanostructures, which is considered as a desirable configuration for sensors due to their simplicity in synthesis, high reproducibility, and excellent compatibility to the well-established semiconductor fabrication processes.[28,29] Although highly sensitive detection of various gases using sensors based on porous thin film with nanostructures has been reported,[30–32]

[a]*Fujian Maternity and Child Health Hospital, Affiliated Hospital of Fujian Medical University, 350001, China*

[b]*Shenzhen Key Laboratory of Advanced Thin Films and Applications, College of Physics and Optoelectronic Engineering, Shenzhen University, 518060, Shenzhen, China. E-mail: luojt@szu.edu.cn*

[c]*School of Materials Science and Engineering, State Key Laboratory of Powder Metallurgy, Central South University, Changsha 410083, China*

† These authors have equal contribution.

so far, the systematically research on the detection of ppb-level NO using porous ZnO nanostructures thin film in the environment with various temperature and humid has not been studied yet.

In this work, we report NO sensors possessing enhanced performance using ZnO nanospirals fabricated by facile and efficient GLAD. The porous ZnO nanospirals with high surface-to-volume ratios present remarkably high sensitivity and selectivity to NO at 150–300 °C even in high RH of 80%. Our ZnO nanospirals sensor system can detect the NO concentration as low as 10 ppb which is below the one (>30 ppb) in exhaled breath of patients with asthma, indicating the great potential for the application in breath analyzers.

Experimental section

ZnO thin film deposition

ZnO nanospiral thin film with the thickness of 400 nm was deposited using the traditional RF magnetic sputtering by GLAD method. To fabricate gas sensors, alumina ceramic plates with the dimension of 10 × 10 × 0.5 mm pre-patterned with inter-digital Ag electrodes were used as the substrates. A metallic zinc target (99.99% pure and 3 inch in diameter) was sputtered in a reactive gas mixture (50% O_2 + 50% Ar) under a pressure of 50 mT at a power of 200 W. The target to substrate distance was kept to be 5.5 cm. The angle θ between the normal vector to the substrate and the incident flux was set at 85° with the deposition rate of 12 nm min^{-1} and the rotation rate of 0.5 rpm. To compare with ZnO nanospiral films, a dense ZnO thin film with the same thickness was also prepared using on-axis RF sputtering.

Microstructure and gas sensing properties characterization

The microstructure of the films was characterized by X-ray diffraction (XRD) measurements using a Cu Kα radiation with $\lambda = 1.5408$ Å. High Resolution Transmission Electron Microscope (HRTEM) images were obtained using JEOL 2100F microscope with an accelerating voltage of 200 kV. The morphologies of the deposited films were characterized using a scanning electron microscope (SEM, Zeiss Supra 55). Photoluminescence (PL) spectrometer, using He–Cd laser as the excitation source, was operated at 325 nm in the air at room temperature to study the crystalline quality and defects of nanospiral and dense ZnO films. After deposition, ZnO thin films were annealed at 400 °C for 2 hours. Gas-sensing properties of the fabricated ZnO thin film sensor were evaluated using an intelligent gas-sensing analysis system. The sensor was put into the test chamber where the temperature was control by an external heating system and the chamber was initially filled with N_2 gas. When the resistance of the sensor became stable, target gas NO (purity of 99.9%) with desired concentrations flowed into the chamber. The change of the sensor resistance was monitored by the intelligent gas-sensing analysis system. After the sensor resistance reached a constant value, it was then recovered by inducing ambient N_2 gas into the chamber. The response of the gas sensor is defined as:

$S = R_{gas}/R_{ambient}$ for NO, or $S = R_{ambient}/R_{gas}$ for CH_4, NH_3, CO and H_2, which was determined by measuring the baseline resistances of the sensors in ambient atmosphere and the fully saturated resistances after exposure to the test gas.

The response time was defined as the time taken by the sensor to achieve the total resistance change in the case of gas adsorption. Similarly, the recovery time was defined as the time taken for the resistance to return back to the baseline. It is found that the working temperature and relative humidity (RH) play important role in the gas sensing performances. The sensors show good selectivity to NO and good long-term stability in N_2 ambient.

Results and discussion

Characterizations of deposited ZnO films

Fig. 1 shows the XRD patterns of the deposited nanospiral and dense ZnO films. For the dense ZnO film, only reflections corresponding to (002) and (004) plane of ZnO located at ~34° and ~72° are observed, indicating growth in a preferred orientation with its *c*-axis normal to the substrate. Besides reflections corresponding to (002) and (004) plane of ZnO, some minor reflection peaks around 31.6° and 36.2° can be found for ZnO nanospiral, which correspond to (100) and (101) plane of ZnO, respectively. Moreover, the XRD intensity of dense ZnO film for (002) plane is stronger than that of ZnO nanospiral. It is suggested that the dense ZnO film has good crystallinity with its *c*-axis normal to the substrate and ZnO nanospiral has (100) and (101) plane besides (002) and (004) plane because of the glancing angle deposition. A comparison of the full-width at half-maximum (FWHM) values of (002) peak intensities of dense ZnO film and ZnO nanospiral thin film show an decease in crystallinity by a 0.1° decrease in the FWHM value.

Fig. 2 shows the room PL spectra of nanospiral and dense ZnO films. The typical ZnO emission peaks located at around 380 nm in ultraviolet (UV) region for nanospiral and dense ZnO films can attributed to the free exciton emissions near band edges for wide band gap of ZnO. Comparing to nanospiral ZnO

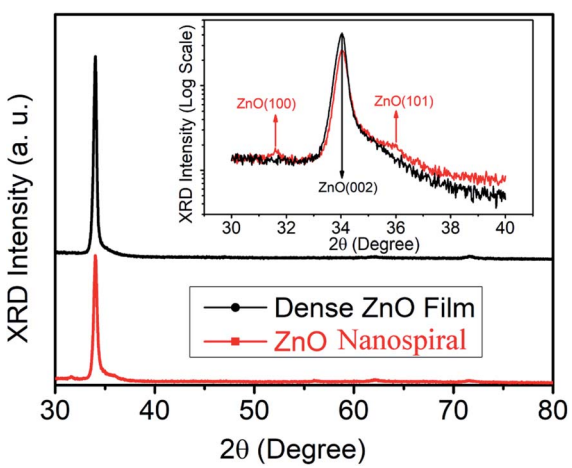

Fig. 1 XRD patterns of nanospiral and dense ZnO thin film. The inset shows the detail of the XRD pattern with 2θ from 30 and 40 degree.

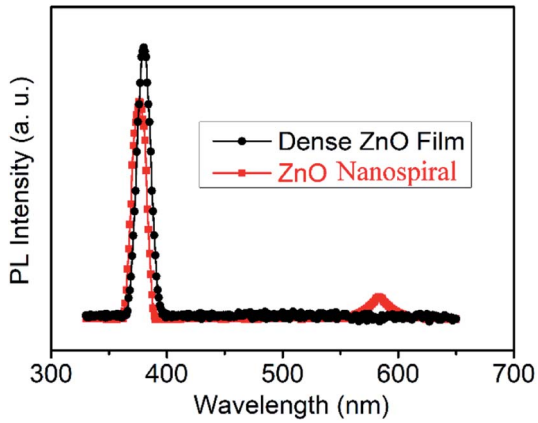

Fig. 2 Room temperature PL spectra of deposited dense and nanospiral ZnO films.

films, dense ZnO films show relatively sharper and stronger UV emission peak, confirming better crystalline quality of the grown films as discussed in XRD patterns. In addition to NBE emission, one broad deep-level (DL) emission peak centred at around 580 nm can be found for nanospiral ZnO films. The DL emission band which lies in the visible region of spectrum has been attributed to the oxygen and zinc vacancies. As shown in the inset of Fig. 1, it can be observed that nanospiral ZnO films have (100) and (101) plane besides (002) and (004) plane because of the glancing angle deposition, which increase the nature and concentration of oxygen and zinc vacancies.

To characterize the microstructure of the nanospiral and dense ZnO films, SEM was used to observe the cross-sectional morphologies of ZnO films. Fig. 3a shows the dense ZnO films with typical compact columnar structure, while nanospiral ZnO films exhibits nanospiral-like structure with large specific surface area (Fig. 3b). To further investigate the details of the microstructure, HRTEM was used to observe the cross-sectional morphologies of the nanospiral ZnO films in a microscopic region. A porous ZnO thin film nanostructures that look similar to the chicken intestinal villi was shown in Fig. 3c. These observations suggest that the porous nanospiral ZnO thin films with high specific surface area were obtained in our work.

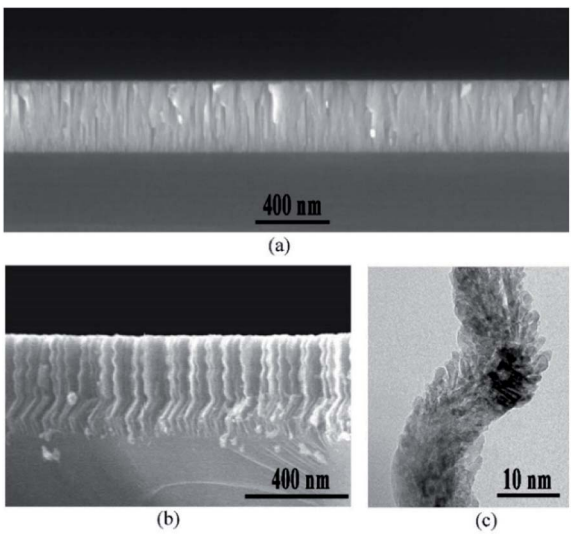

Fig. 3 Cross-sectional morphologies of nanospiral and dense ZnO thin film. (a) SEM images of the cross-sectional view of dense ZnO films. (b) SEM images of the cross-sectional view of nanospiral ZnO thin film. (c) HRTEM images of a small area of nanospiral ZnO.

Gas sensing properties

The NO gas sensing performance of nanospiral and dense ZnO thin films were investigated. Fig. 4 shows the repetitive cycles of resistance variation of the sensors as they were exposed to NO gas with a fixed concentration of 100 ppb at 150 °C with 40% of RH in N_2 ambient. For nanospiral ZnO thin film, initially, the sensor showed a resistance around 1 MΩ. After NO target gas was pumped into the test chamber (*i.e.*, the adsorption of gas on the sensor surface), the resistance increased rapidly and reached a saturated value over 17.5 MΩ. Then the NO gas was stopped and followed by the ambient N_2 gas, the resistance gradually returned to its original value. The response and recovery times of the sensors are around 50 s and 500 s, respectively. For comparison, the sensor based on dense ZnO thin film shows an increase of the resistance to 6 MΩ after NO injection. The response and recovery times of the dense ZnO thin film sensor are around 60 s and 1100 s, respectively. The responses of nanospiral and dense ZnO thin film sensors to 100 ppb of NO gas at 150 °C under 40% of RH in N_2 ambient

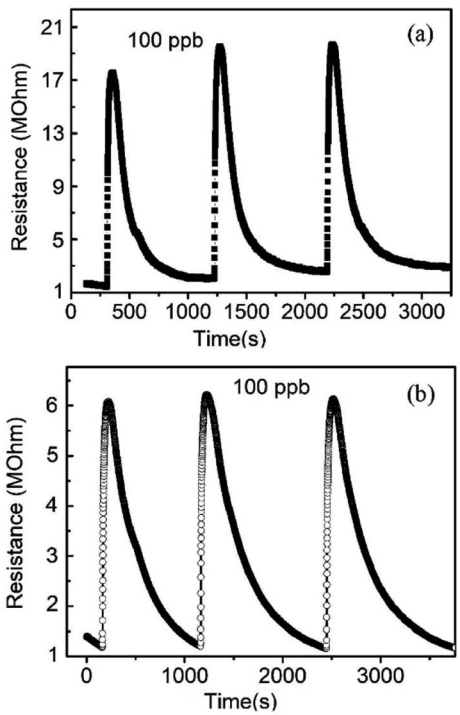

Fig. 4 The resistance changes of the sensors based on (a) nanospiral and (b) dense ZnO thin film when exposed to NO with 100 ppb at 150 °C under 40% in N_2 ambient.

were calculated to be 16.9 and 5.2, respectively. Compared to dense ZnO thin film sensor, the sensor based on porous nanospiral ZnO thin films showed better NO sensing performance with higher response (resistance change), faster response and recovery speeds. The sensor exhibited a good reproducibility after repeated testing cycles, as the sensor showed a nearly constant amplitude of the initial response without any obvious change after consecutively three tests expose to the same NO concentration.

The response performance of the porous nanospiral ZnO thin films sensor corresponding to different NO concentrations of 70, 80 and 90 ppb at 150 °C under 40% of RH in N_2 ambient is shown in Fig. 5a. The resistance increased immediately after exposed to the NO gas and recovered completely after pumped in the ambient gas, showing good reproductive when the sensor was tested at different NO concentrations. Therefore, the porous ZnO nanospiral thin film is capable for reusable sensor in highly stable operation. The sensor response increases linearly with the increasing NO concentration, which is a basic feature for sensors based on n-type semiconductor. In order to estimate the NO experimental detection limit of the ZnO thin film sensors, NO concentrations of 5, 10, 20, 30, 40, 50 and 60 ppb at 150 °C under 40% of RH in N_2 ambient were used in our experiments to test the response of nanospiral and dense ZnO films as shown in Fig. 5b. The porous ZnO nanospiral thin film sensor does not respond to 5 ppb NO, but concentration higher than 10 ppm is readily detected. Even with concentration of 10 ppb, the porous ZnO nanospiral thin film sensor shows a clear response of 2.5. On the other hand, dense ZnO thin film sensor can only detect NO gas with the concentration over 40 ppb. The linear relationship between the response value and the gas concentration demonstrates the feasibility and the operation capability of the sensors for real human breath diagnostic application.

Fig. 6a shows that the response values depend on the working temperature (range from 100 to 300 °C) of the sensors based on nanospiral and dense ZnO thin films exposed to NO gas of 90 ppb under 40% RH in N_2 ambient. It shows that the working temperature has a great impact on the response of the

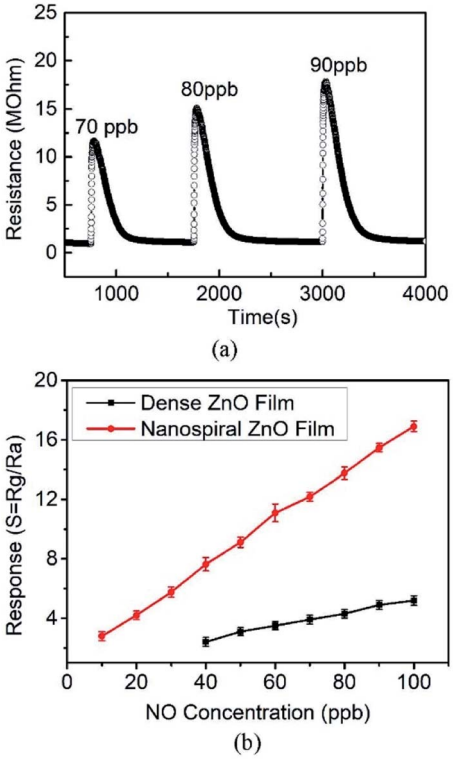

Fig. 5 (a) The resistance changes of the sensors based on nanospiral ZnO thin film when exposed to NO gas with 70, 80, 90 ppb at 150 °C under 40%. (b) The responses changes of the sensors based on nanospiral and dense ZnO thin film when exposed to NO with different concentration at 150 °C under 40%.

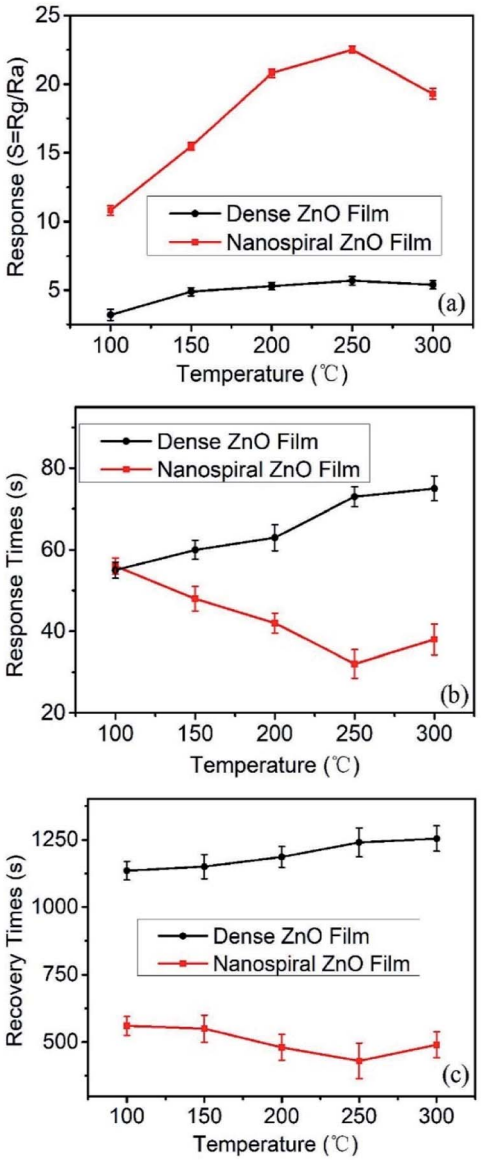

Fig. 6 (a) The response, (b) response and (c) recovery times of the sensors based on nanospiral and dense ZnO thin films exposure to NO gas of 90 ppb under 40% RH in N_2 ambient at different working temperature (range from 100 to 300 °C).

sensors. For sensors based on nanospiral ZnO thin films, the response increases rapidly with the increase of working temperature and reaches a maximum value of ~23 at 250 °C, then decreases gradually as the working temperature increases further. On the other hand, although the responses also increases with the increase of working temperature, the influence of the working temperature on the sensor based on dense ZnO thin films is not as much as that of the sensor based on nanospiral ZnO thin films. The sensing process is a dynamic balance of diffusion, adsorption, reaction and desorption of NO molecules on the ZnO surface and nanostructure interface. Increased working temperature will accelerate the diffusion and reaction between NO molecules and ZnO films, and depress the adsorption. This acceleration will be enhanced by the porous nanospiral ZnO thin films. However, higher temperature (>250 °C) will cause a large amount of oxygen molecules dissociate and adsorb on the active sites, resulting in the decrease of the free active sites for the adsorption of NO, which cause the decrease of the sensor's response.

The kinetic performance of the NO gas sensing depends on the working temperature of the sensors, which can be characterized by the response and recovery times. Fig. 6b and c present the response and recovery time of the sensors based on nanospiral and dense ZnO film depending on the working temperature ranging from 150 to 300 °C. It is found that nanospiral ZnO films show faster response and recovery speed than that of dense ZnO thin film in the temperature range of 150–300 °C, and the sensors based on nanospiral ZnO films show the fastest response and recovery at the working temperature of 250 °C. These results can be explained by the gas diffusion and the reaction on the surface of ZnO thin films. The gas diffusion strongly depends on the porosity, the relative surface area and the active surfaces and interface. The nanospiral ZnO thin films provide porous characteristics and large relative surface area, which are favourable for the rapid diffusion of gas molecules and also provide more active surface. Moreover, the increase of the working temperature will accelerate the diffusion, the adsorption, the reaction and desorption of NO gas on the nanospiral ZnO thin film, resulting in the highest rates of the response and recovery speed at 250 °C. Therefore, the response value, the response/recovery speed, the performance of the sensor based on nanospiral ZnO thin film working at 250 °C has been optimised.

As for breath analysis application, the anti-interference ability of NO sensors based on nanospiral ZnO thin film to NH_3, CH_4, H_2 and CO, which usually exist in exhaled human breath, should be considered. Selectivity histogram for the NO sensors based on nanospiral ZnO thin film was investigated by exposing the gas sensors to different types of gases with a fixed concentration of 90 ppb, including NO, NH_3, CH_4, H_2 and CO at the working temperature of 150 °C under 40% RH in N_2 ambient, which is shown in Fig. 7. Obviously, the sensor exhibits the highest response to NO gas compared to other interference gases, indicating a very good selectivity. The selectivity of the sensor against NO could be attributed to lower activation energy of ZnO thin film against NO, which accelerates the desorption reactions and enhances the NO sensing

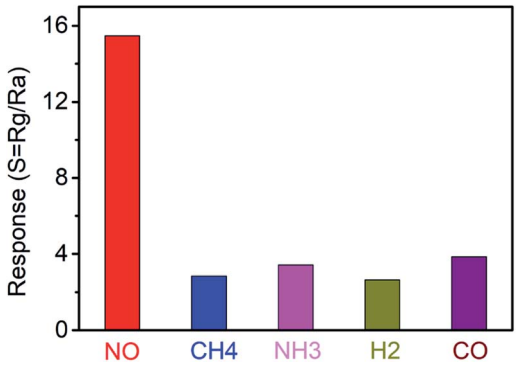

Fig. 7 The anti-interference ability of NO sensors based on nanospiral ZnO thin film to NH_3, CH_4, H_2 and CO.

performance compared to other gases. For working temperature of 150 °C, there are much less ionized oxygen species on the surface of ZnO. Therefore, reducing gases such as NH_3, CH_4, H_2 and CO have a poor sensitivity at this temperature.

For exhaled breath application, normally the sensor should work in a highly humid environment (RH > 80%). Therefore, the gas sensing performance of the ZnO film sensor exposed to 90 ppb NO gas working at the temperature of 150 °C were investigated with different humidity conditions. The RH values were controlled by filling N_2 gas flow passing through saturated aqueous solutions of different salts of CH_3COOK, $Mg(NO_3)_2$, $NaNO_3$, and KNO_3, yielding 20%, 40%, 60% and 80% RH, respectively. The dependence of the response, the response and recovery time on the RH were shown in Fig. 8a–c, respectively. It is found that the response decreases and the response and recovery time increases with the increasing of RH for both nanospiral and dense ZnO thin film sensors. This is because water molecules adsorbed on the surface of ZnO films at high RH, occupying the active sites and blocking off the apertures.[33] Therefore, the adsorption and the diffusion of NO molecules were interfered by water molecules, resulting in lower and slower sensor response. However, even with RH value as high as 80% at the working temperature of 150 °C, nanospiral ZnO thin film sensors exposed to 90 ppb NO gas still have response as high as 14 with the response time and recovery time of 60 s and 700 s, respectively.

To evaluate the long-term stability of the sensor in N_2 ambient conditions, we conducted the stability measurement of nanospiral and dense ZnO thin film sensors in continuous operation for more than 20 days at 150 °C under 40% RH in N_2 ambient. The sensors were relatively stable with a variation below 5% of the response after repeated exposure to 90 ppb of NO gas over 20 days (Fig. 9), which might due to the air-stability of the nanospiral and dense ZnO thin film itself.

NO gas-sensing mechanism

NO gas-sensing mechanism can be understood based on the resistance change resulted from the adsorption of NO gas molecules onto nanospiral and dense ZnO thin film, and the

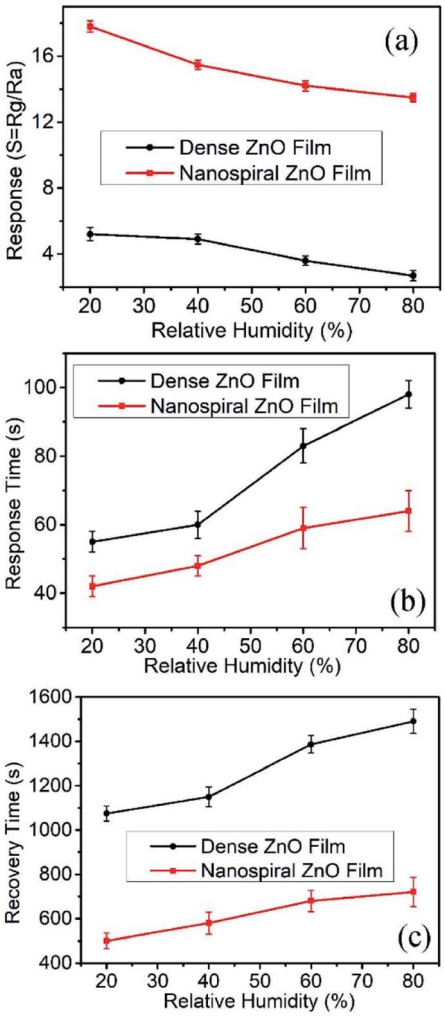

Fig. 8 The response, response and recovery times of the sensors based on nanospiral and dense ZnO thin films exposure to NO gas of 90 ppb at 150 °C under different RH in N_2 ambient.

reaction between them.[34] The possible reactions on the surface of the ZnO thin films can be described as following:[35–38]

$$O_{2(gas)} + e^- \rightarrow O_2^-{}_{(ads)} \quad (1)$$

$$\tfrac{1}{2}O_{2(gas)} + e^- \rightarrow O^-{}_{(ads)} \quad (2)$$

$$O^-{}_{(ads)} + e^- \rightarrow O^{2-}{}_{(ads)} \quad (3)$$

$$NO_{(gas)} + O_2^-{}_{(ads)} + e^- \rightarrow NO_2^-{}_{(ads)} + O^-{}_{(ads)} \quad (4)$$

$$NO_{(gas)} + O_{ads}^- \rightarrow NO_{2(gas)} + e^- \quad (5)$$

$$NO_{(gas)} + e^- \rightarrow NO^-{}_{(ads)} \quad (6)$$

$$NO^-{}_{(ads)} + O_2^-{}_{(ads)} + 2e^- \rightarrow NO_{(gas)} + O^-{}_{(ads)} \quad (7)$$

$$2NO_{(gas)} + 2e^- \rightarrow N_{2(gas)} + 2O^-{}_{(ads)} \quad (8)$$

The possible reactions mentioned above include the adsorption and desorption of oxygen molecules as well as the surface response to NO, NO^-, and NO_2^- adsorption. Due to the oxygen and zinc vacancies exist in ZnO thin film, oxygen molecules adsorb on the surface of ZnO thin film. Because of their electronegativity, the adsorbed oxygen molecules trap electrons from the conduction band of ZnO thin film, which thus causes the formation of oxygen species such as $O_2^-{}_{(ads)}$, $O^-{}_{(ads)}$ and $O^{2-}{}_{(ads)}$ on the surface of ZnO thin films. Because of the electron trapping from ZnO thin film, the population of electrons as major free charge carriers is lowered, which results in the formation of a depletion region on the surface layer of ZnO thin films. Therefore, the charge carrier concentration decreases and the resistance of ZnO thin films increases. The molecular NO_x has an unpaired electron and is known as a strong oxidizer than other gases.[9] When exposed to NO gas, the active sites on the surface of ZnO thin film were occupied by NO molecules, which thickens the depletion layer *via* capturing electrons from the conduction band ZnO thin film and generates NO^-, NO^{2-} and O^{2-}.[35] These nitrite and/or nitrate species can also be result from the reactions between NO molecules and oxygen species on the surface of ZnO films. Consequently, the total resistance of the sensor is further increased. Compared to dense ZnO thin film sensor, there are some reasons for nanospiral ZnO thin film sensor possess better sensing performance. Firstly, porous nanospiral ZnO thin film with high surface to volume ratios can provide more active adsorption sites, hence higher response values. Secondly, nanospiral ZnO thin film exhibits (100) and (101) crystal plane and broad DL emission peak, demonstrating more oxygen and zinc vacancies, which enhances the absorption and reaction of NO gas on the surface. Moreover, porous nanospiral ZnO thin film provide lots of gas channel to accelerate the diffusion and desorption of NO, resulting in the high response and recovery speed. The improvement of sensing performance by constructing nanostructures has also been successfully reported in mesoporous ZnO nanosheets, atomically thin-layered MoS_2, WS_2 nanosheets, *etc.*[39–42]

A comparative table about the sensor performance of this work with some other NO sensors is shown in Table 1. Most of

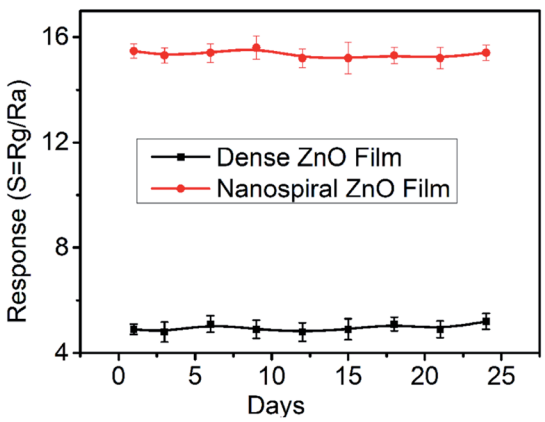

Fig. 9 The long-term stability of the sensors based on nanospiral and dense ZnO thin films when exposure to NO gas of 90 ppb at 150 °C under 40% RH.

Table 1 Performance of NO sensors based on different sensing materials

Material	NO (ppm)	Response	Working temperature (°C)	LOD (ppb)	Humidity (RH%)	t_{Resp}/t_{Reco} (s)	Ref.
Villi-like WO_3	1	275	200	0.08	80	100/20	9
0.1Pd–WO_3	20	164.4	200	—	—	185/400	37
ZnO nanobelt	50	6.5	28	500	—	200/250	43
ZnO/CdO (2.8 : 1) nanofibers	3	1.7	215	1200	Ignorable	47/1249	38
ZnO nanofibers	12	7	200	—	—	400/1200	44
In_2O_3–ZnO	10	8	100	12	—	210/2700	45
Nanospiral ZnO	0.09	14	150	10	80	60/700	This work
Dense ZnO	0.09	2	150	40	80	∼100/∼1500	This work

the sensors works at high NO concentration and shows large limit of detection (LOD). Few investigations on the effect of humidity on the sensing performance have been reported. Although the sensors reported in our work shows relatively good sensitivity, long-term stability and reproducibility, the response and recovery speed needs improvement in our future work.

Conclusions

In this work, we have proposed a facile technique to fabricate NO gas sensor with excellent sensing performance based on nanospiral ZnO thin film deposited by GLAD. Nanospiral ZnO thin film exhibits (100) and (101) crystal plane and broad DL emission peak, demonstrating more oxygen and zinc vacancies, which enhances the absorption and reaction of NO gas on the surface. Moreover, the porous and nanospiral-like characteristic provides more active sites for NO absorption and the reaction between NO gas and ZnO thin film, and also accelerates the diffusion and desorption, which ensure the large response and response and recovery speed. Even upon exposure to 10 ppb NO at 150 °C under 40% RH in N_2 ambient, the nanospiral ZnO thin film sensor still showed a clear response of 2.5. The response increased and the response and recovery time decreased with the increasing humidity. However, even with RH value as high as 80%, nanospiral ZnO thin film sensors still presented a response as high as 14 with a response and recovery time of 60 s and 700 s, respectively. Moreover, we demonstrated that the nanospiral ZnO thin film sensor had good selectivity to NO and high stability in operation for over 20 days. Since NO is a well-known biomarker of chronic airway inflammation in asthma, ZnO nanospiral sensor fabricated by facile and efficient GLAD has a great potential for the use in breath analysis.

Conflicts of interest

There are no conflicts to declare.

Acknowledgements

The authors gratefully acknowledge the support of Research and Development Program of China (Grant no. 2016YFB0402705), Shenzhen Science & Technology Project (Grant no. JCYJ20180507182106754, JCYJ2018050718243957, JCYJ20180305124317872).

References

1 S. L. Bai, H. Fu, Y. Y. Zhao, K. Tian, R. X. Luo, D. Q. Li and A. Chen, *Sens. Actuators, B*, 2018, **266**, 692–702.
2 S. C. Anenberg, J. Miller, R. M. Injares, L. Du, D. K. Henze, F. Lacey, C. S. Malley, L. Emberson, V. Franco, Z. Kilmont and C. Heyes, *Nature*, 2017, **545**, 467–471.
3 M. Li, J. T. Luo, C. Fu, H. Kan, Z. Huang, W. M. Huang, S. Q. Yang, J. B. Zhang, J. Tang, Y. Q. Fu, H. L. Li and H. Liu, *Sens. Actuators, B*, 2018, **256**, 1045–1056.
4 T. Samerjai, D. Channei, C. Khanta, K. Inyawilert, C. Liewhiran, A. Wisitsoraat, D. Phokharatkul and S. Phanichphant, *J. Alloys Compd.*, 2016, **680**, 711–721.
5 Y. Qin, C. Liu, M. Liu and Y. Liu, *J. Alloys Compd.*, 2014, **615**, 616–623.
6 O. Kuzmych, B. L. Allen and A. Star, *Nanotechnology*, 2007, **18**, 375502.
7 J. Jyoti and G. D. Varma, *J. Alloys Compd.*, 2019, **806**, 1469–1480.
8 E. Tseliou, V. Bessa, G. Hillas and V. Del, *Chest*, 2015, **138**, 107–113.
9 H. G. Moon, Y. R. Choi, Y. S. Shim, K. I. Choi, J. H. Lee, J. S. Kim, S. J. Yoon, H. H. Park, C. Y. Kang and H. W. Jang, *ACS Appl. Mater. Interfaces*, 2013, **5**, 10591–10596.
10 S. P. Mondal, P. K. Dutta, G. W. Hunter, B. J. Ward, D. Laskowski and R. A. Dweik, *Sens. Actuators, B*, 2011, **158**, 292–298.
11 B. Buszewski, M. Kesy, T. Ligor and A. Amann, *Biomed. Chromatogr.*, 2007, **21**, 553–566.
12 M. Righettoni, A. Tricoli and S. E. Pratsinis, *Anal. Chem.*, 2010, **82**, 3581–3587.
13 J. Shin, S. Choi, I. Lee, D. Youn, C. Park, J. Lee, H. Tuller and I. Kim, *Adv. Funct. Mater.*, 2013, **23**, 2357–2367.
14 P. Spane, K. Dryahina and D. J. Smith, *J. Breath Res.*, 2007, **1**, 011001.
15 J. D. Prades, A. Cirera, J. R. Morante, J. M. Pruneda and P. Ordejon, *Sens. Actuators, B*, 2007, **126**, 62–67.
16 M. Ali, Ch. Y. Wang, C. C. Rohlig, V. Cimalla, Th. Stauden and O. Ambacher, *Sens. Actuators, B*, 2008, **129**, 467–472.

17 S. P. Mondala, P. K. Dutta, G. W. Hunter, B. J. Ward, D. Laskowski and R. A. Dweik, *Sens. Actuators, B*, 2011, **158**, 292–298.
18 H. Xia, Y. Wang, F. Kong, S. Wang, B. Zhu, X. Guo, J. Zhang, Y. Wang and S. Wu, *Sens. Actuators, B*, 2008, **134**, 133–139.
19 C. Sun, G. Maduraiveeran and P. Dutta, *Sens. Actuators, B*, 2013, **186**, 117–125.
20 D. Velasco-Arias, D. Diaz, P. Santiago-Jacinto, G. Rodríguez-Gattorno, A. Vazquez-Olmos and S. E. Castillo-Blum, *J. Nanosci. Nanotechnol.*, 2008, **8**, 6389–6394.
21 S. Barth, R. Jimenez-Diaz, J. Sama, J. D. Prades, I. Gracia, J. Santander, C. Canec and A. Romano-Rodriguez, *Chem. Commun.*, 2012, **48**, 4734–4736.
22 W. Li, X. Geng, Y. Guo, J. Rong, Y. Gong, L. Wu, X. Zhang, P. Li, J. Xu, G. Cheng, M. Sun and L. Liu, *ACS Nano*, 2011, **5**, 6955–6961.
23 I. D. Kim, A. Rothschild and H. L. Tuller, *Acta Mater.*, 2013, **61**, 974–1000.
24 H. Liu, M. Li, O. Voznyy, L. Hu, Q. Fu, D. Zhou, Z. Xia, E. H. Sargent and J. Tang, *Adv. Mater.*, 2014, **26**, 2718–2724.
25 Z. F. Huang, J. Song, L. Pan, X. Zhang, L. Wang and J. J. Zou, *Adv. Mater.*, 2015, **27**, 5309–5327.
26 M. W. Ahn, K. S. Park, J. H. Heo, D. W. Kim, K. J. Choi and J. G. Park, *Sens. Actuators, B*, 2019, **138**, 168–173.
27 S. C. Navale, V. Ravi, I. S. Mulla, S. W. Gosavi and S. K. Kulkarni, *Sens. Actuators, B*, 2007, **126**, 382–386.
28 S. V. Kesapragada, P. Victor, O. Nalamasu and D. Gall, *Nano Lett.*, 2006, **6**, 854–857.
29 M. M. Hawkeye and M. J. Brett, *J. Vac. Sci. Technol.*, 2017, **25**, 1317.
30 M. W. Ahn, K. S. Park, J. H. Heo, D. W. Kim, K. J. Choi and J. G. Park, *Sens. Actuators, B*, 2009, **138**, 168–173.
31 L. Liao, H. B. Lu, M. Shuai, J. C. Li, Y. L. Liu, C. Liu, Z. X. Shen and T. Yu, *Nanotechnology*, 2008, **19**, 175501.
32 H. G. Moon, Y. S. Shim, D. H. Kim, H. Y. Jeong, M. H. Jeong, J. Y. Jung, S. M. Han, J. K. Kim, J. S. Kim, H. H. Park, J. H. Lee, H. L. Tuller, S. J. Yoon and H. W. Jang, *Sci. Rep.*, 2012, **2**, 588.
33 H. L. Tian, H. Q. Fan, G. Z. Dong, L. T. Ma and J. W. Ma, *RSC Adv.*, 2016, **6**, 109091–109098.
34 N. Yamazoe, *Sens. Actuators, B*, 1991, **5**, 7–19.
35 A. Afzal, N. Cioffi, L. Sabbatini and L. Torsi, *Sens. Actuators, B*, 2012, **171**, 25–42.
36 X. Bao, U. Wild, M. Muhler, B. Pettinger, R. Schlogl and G. Ertl, *Surf. Sci.*, 1999, **425**, 224–232.
37 Z. X. Cai, H. Y. Li, J. C. Ding and X. Guo, *Sens. Actuators, B*, 2017, **246**, 225–234.
38 H. Naderi, S. Hajati, M. Ghaedi and J. P. Espinos, *Sens. Actuators, B*, 2019, **297**, 126774.
39 S. P. Gupta, A. S. Pawbake, B. R. Sathe, D. J. Late and P. S. Walke, *Sens. Actuators, B*, 2019, **293**, 83–92.
40 X. B. Ren, K. Ren, Y. Zhang, C. G. Ming and Q. Han, *Beilstein J. Nanotechnol.*, 2019, **10**, 467–474.
41 D. J. Late, Y. K. Huang, B. Liu, J. Acharya, S. N. Shirodkar, J. J. Luo, A. Yan, D. Charles, U. V. Waghmare, V. P. Dravid and C. N. R. Rao, *ACS Nano*, 2013, **7**, 4879–4891.
42 D. J. Late, R. V. Kanawade, P. K. Kanan and C. S. Rout, *Sens. Lett.*, 2016, **14**, 1249–1254.
43 S. K. M. Kaur, N. Ramgir, N. Datta, S. Kumar, A. K. Debnath, D. K. Aswal and S. K. Gupta, *Appl. Surf. Sci.*, 2017, **394**, 258–266.
44 O. K. Kim, H. Kim and D. Kim, *Korean J. Mater. Res.*, 2012, **22**, 609–614.
45 C. Y. Lin, Y. Y. Fang, C. W. Lin, J. J. Tunney and K. C. Ho, *Sens. Actuators, B*, 2010, **146**, 28–34.